PAPER

Interaction between interstitial carbon atoms and a ½ 〈1 1 1〉 self-interstitial atoms loop in an iron matrix: a combined DFT, off lattice KMC and MD study

To cite this article: R Candela *et al* 2018 *J. Phys.: Condens. Matter* **30** 335901

IOP Publishing Journal of Physics: Condensed Matter

J. Phys.: Condens. Matter **30** (2018) 335901 (15pp) https://doi.org/10.1088/1361-648X/aad25d

Interaction between interstitial carbon atoms and a ½ ⟨1 1 1⟩ self-interstitial atoms loop in an iron matrix: a combined DFT, off lattice KMC and MD study

R Candela[1,2], N Mousseau[3], R G A Veiga[4], C Domain[2,5] and C S Becquart[1,2]

[1] Univ. Lille, CNRS, INRA, ENSCL, UMR 8207, UMET, Unité Matériaux et Transformations, F 59 000 Lille, France
[2] Laboratoire commun EDF-CNRS Etude et Modélisation des Microstructures pour le Vieillissement des Matériaux (EM2VM), France
[3] Département de physique and Regroupement québécois sur les matériaux de pointe, Université de Montréal, Case postale 6128, succursale centre-ville, Montreal, QC H3C 3J7, Canada
[4] Universidade Federal do ABC, Center for Engineering, Modeling, and Social Applied Sciences (CECS), Av. dos Estados, 5001, Santa Terezinha, CEP 09210-580, Santo André/SP, Brazil
[5] EDF-R&D, Département Matériaux et Mécanique des Composants (MMC), Les Renardières, F-77818 Moret sur Loing Cedex, France

E-mail: charlotte.becquart@univ-lille1.fr

Received 22 March 2018, revised 4 July 2018
Accepted for publication 10 July 2018
Published 30 July 2018

Abstract

A static and kinetic study of the interaction between a 19 ½ ⟨1 1 1⟩ self-interstitial atoms loop and C atoms in body-centred cubic iron is presented in this work. An empirical potential matching the density functional theory calculations is used to study the static properties of the system. The usual kinetic Monte-Carlo (KMC) on-lattice restriction is not valid when the material is highly distorted, especially in the presence of a dislocation loop. Therefore, the dynamics of the system are investigated using both molecular dynamics simulations and k-ART, a self-learning/off-lattice atomic kinetic Monte-Carlo. The presented work is thus a full study of the C-loop and the C2-loop systems. A good agreement is observed between the statics and the kinetics (e.g. the discovery of a zone of stability of the C atom around the Fe cluster where the C can almost freely move), even though the kinetics show some unexpected behaviours of the studied systems. The pinning time of the loop induced by the C atoms is also estimated.

Keywords: dislocation loop, molecular dynamics, irradiation, BCC steels, off-lattice kinetic Monte-Carlo, DFT

Supplementary material for this article is available online

(Some figures may appear in colour only in the online journal)

1. Introduction

Body-centred cubic (bcc) iron alloys are typically used in the nuclear industry, especially for reactor pressure vessels. Due to the high formation energy of self-interstitial atoms (SIA) in iron, defects such as SIA dislocation loops are found in materials that have been exposed to irradiation such as neutron irradiation: the concerned Fe–C alloys are the nuclear reactor vessel and the nuclear reactor internal parts. ½ ⟨1 1 1⟩ dislocations loops are known to have a very low migration

energy along the ⟨1 1 1⟩ direction [1] in pure Fe thus making it a mobile defect which can easily interact with other defects, as presented in the mechanism proposed by Xu *et al* leading to the formation of ⟨1 0 0⟩ loops by the interaction between two ½ ⟨1 1 1⟩ loops [2]. While the very mobile ⟨1 1 1⟩ loops may migrate to grain boundaries, the almost immobile ⟨1 0 0⟩ loops are expected to accumulate in the microstructure and act as sinks for mobile defects [2] and may as well hinder the dislocations movement. Therefore, quantifying the change of mobility of ⟨1 1 1⟩ loops due to the C atoms is of primary importance to have a better understanding of the evolution of the microstructure of irradiated steels. The addition of alloying elements in pure bcc Fe matrix has an influence on the loop mobility. Arakawa *et al* observed a lowering in the loop motion due to Cr segregation at the loop periphery for temperatures above 450 K [3]. As for interstitial impurities, the presence of even very small amount of carbon affects properties of Fe and Fe-based ferritic alloys. This comes from the fact that carbon exhibits strong interaction with lattice defects—see for instance [4]—and therefore influences their mobility [5], thus affecting the evolution of the microstructure. As an example, the strong affinity of carbon with vacancies in α-Fe leads to the formation of carbon–vacancy (*C–V*) complexes that can trap SIA loops [6]. Indeed, molecular dynamics (MD) simulations showed that *v–C* and *v–C*2 complexes can be responsible for the slowing down or even the complete stopping of ½ ⟨1 1 1⟩ SIA clusters [7]. The same authors showed that C decorated loops acted as strong obstacles for dislocations [8]. A single carbon atom was shown to hinder the movement of dislocations [9, 10] or ⟨1 0 0⟩ dislocation loops [8] in Fe, whereas Khater *et al* [11] showed that the stress level at 0 K due to a solid solution of C around an edge dislocation is lower than the Peierls stress leading to a softening of the material. On the contrary, these C atoms will tend to migrate towards the dislocation thus creating a well-known Cottrell atmosphere [12]. In these atmospheres, due to C atoms that occupy pinning positions, the unpinning stress is higher as shown very recently in a study combining Monte Carlo and MD [13].

The aim of this work is to study the interaction between C atom(s) and an ½ ⟨1 1 1⟩ dislocation loop composed of 19 iron SIA (i19 loop) within bcc Fe matrix. The i19 loop is expected to be representative of larger ⟨1 1 1⟩ loops because only the last shell of the loop and the first shell outside the loop are found not to be in a bcc environment [14]. Firstly, the static properties of the system are studied by density functional theory (DFT) and compared with the results of a well-assessed empirical potential [15] in order to determine the stability of the different configurations. This is done by calculating the binding energy between the C atom(s) and the loop. Secondly, the dynamic properties of the system are investigated at different temperatures for the different initial configurations given by the static study of the system. The aim of this dynamic study is to investigate the evolution in time of the loop and the C atom(s). A discussion will summarize the principal results of this work and show the consequences induced by the presence of C atoms near the loop.

2. Method

2.1. DFT calculations

DFT has been used within the projector augmented wave method as implemented in the Vienna *ab initio* simulation package (VASP) [16–19]. The Perdew and Wang [20] parameterization of the generalized gradient approximation has been used. For the spin interpolation of the correlation potential, the improved Vosko–Wilk–Nusair interpolation has been applied. Supercells of 1458 bcc positions ($9 \times 9 \times 9$ bcc two atoms unit cell with a_0 2.831 Å) were used with Gamma point representation of the Brillouin zone as the supercells are large. The plane wave energies were cut off at 300 eV. All the atoms were relaxed under constant volume condition.

The perfect interstitial ⟨1 1 1⟩ loop is introduced in the middle of the supercell and the influence of the pressure due to the use of constant volume has been evaluated using the method proposed by Varvenne *et al* [21] to take into account long range interactions. Once point defect energies have been calculated using VASP, they are corrected by subtracting artifactitious interaction energy arising from periodic boundary conditions. Because the introduction of an i19 ⟨1 1 1⟩ loop can induce a large pressure on the simulation box, the calculations were also done using a box size enlarged by 19 atomic volumes. The new lattice parameter a_{19} was then adjusted to match the new volume of the box. More precisely, this is done as such:

$$a_{19} = \frac{a_0}{N_{\text{box}}} \sqrt[3]{N_{\text{box}}^3 + \frac{19}{2}}$$

where N_{box} is the duplication of the unit cell in each direction ($N_{\text{box}} = 9$ for the DFT calculations).

It was found that these two methods to take into account the pressure applied return results that differ by less than 4% in the binding energies in average thus allowing one to confirm that the addition of 19 atomic volumes in the box is a valid correction. The local magnetic moments are calculated by taking the spin from the charge density difference integrated over spheres on each atom.

2.2. Cohesive model for the empirical potential calculations

Energy minimizations were done using the MD code DYMOKA [22] with simulation boxes of the same size as the ones used in the DFT calculations, i.e. $9 \times 9 \times 9$ boxes (1458 Fe atoms on a bcc lattice) with an i19 loop and a C atom. The empirical potential chosen is the one derived by Becquart *et al* [15] which was slightly modified by Veiga [23]. This Fe–C potential has been previously used to model Fe–C systems, with a particular focus on carbon-dislocation interactions [13, 24, 25] and the dynamics of carbon in bulk Fe[15] [26]. It was also used to model internal friction experiments [27], martensite properties [28], and C ordering in Fe–C crystallites at high C concentrations [29]. Periodic boundary conditions were applied along all the directions and the total energy of the system was minimized on both boxes with and without the correction on the lattice parameter due to the pressure

induced by the introduction of the i19 loop. Just like for DFT relaxation, a difference in the binding energies between the C atom and the loop was observed whether we adjust the lattice parameter or not to take into account pressure added by the addition of the loop.

2.3. Static properties

2.3.1. Binding energy. In a bcc Fe lattice containing N atomic sites, the total binding energy between n objects, i.e. vacancies, self-interstitial atoms, Fe or solute atoms, is the energy difference between the configuration where all the objects interact and the system where all the objects are far enough from one another to not interact anymore. Due to the limited supercell size, the total binding energy is calculated as follows:

$$E_{\mathrm{b}}\left(A_1, A_2, ..., A_n\right) = \sum_{i=1,...,n} E\left(A_i\right) - \left[E\left(A_1 + A_2 + ... + A_n\right) + (n-1)\, E_{\mathrm{ref}}\right]$$

where E_{ref} is the energy of the supercell without any defects, $E\left(A_i\right)$ is the energy of the supercell with A_i, and $E\left(A_1 + A_2 + ... + A_n\right)$ is the energy of the cell containing all A_i interacting defects. All the supercells contain the same number of lattice sites, i.e. have the same size. More precisely, here are the binding energies for a system containing a loop with a C atom and a loop with two C atoms in a pure Fe matrix respectively, so for the systems studied in this paper:

$$E_{\mathrm{b}}\left(\mathrm{C} - \mathrm{loop}\right) = E\left(\mathrm{C}\right) + E\left(\mathrm{loop}\right) - \left[\left(E\left(\mathrm{C\_and\_loop}\right) + E(\mathrm{perfect\_lattice})\right]$$

$$E_{\mathrm{b}}\left(2\mathrm{C} - \mathrm{loop}\right) = 2 \times E\left(\mathrm{C}\right) + E\left(\mathrm{loop}\right) - \left[\left(E\left(2\ \mathrm{C\_and\_loop}\right) + 2 \times E(\mathrm{perfect\_lattice})\right].$$

With this definition, positive values correspond to binding (or attractive) configurations. The binding energy depicts the attraction/repulsion between the defects and so the overall stability of the system. Indeed, the higher the binding energy between a C atom and the loop, the more stable the configuration.

2.3.2. Distances between the loop centre of mass and the C atom. The loop centre of mass (CM) is defined as the centroid of all the Fe atoms composing the loop, i.e. all Fe atoms that are not close to the perfect bcc lattice. The C-CM distance is not enough to fully describe the carbon environment especially because the same distance may correspond to different configurations. Two variables are thus defined: D(C-CM), the distance between the CM and the C atom projection on the (1 1 1) plane comprising the CM and H(C-CM), the distance between the C atom and the (1 1 1) plane comprising the CM. In the square triangle defined by the C atom, the CM and H the orthogonal projection of the C atom to the (1 1 1) plane comprising the CM, the two variables are D(C-CM) and H(C-CM) are respectively the opposite side and the adjacent side of the right angle. Figure 1 represents these variables for a better understanding.

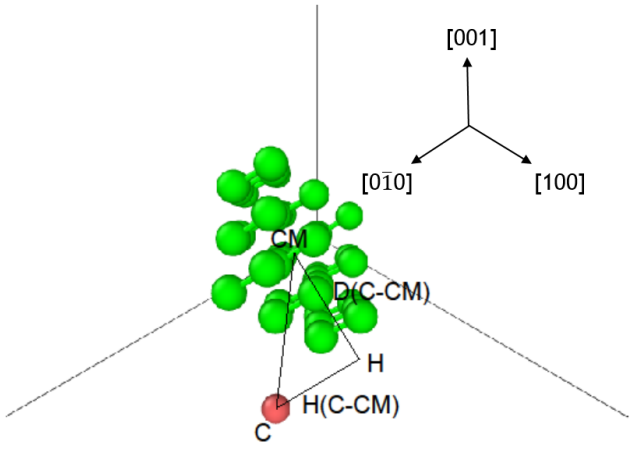

Figure 1. Representation of the variables D(C-CM) and H(C-CM) in the presence of an i19 loop (green atoms) and a C atom (in red) in a pure Fe matrix with CM the loop centre of mass and H the orthogonal projection of C on the (1 1 1) plane containing CM. For the sake of simplicity, the Fe matrix is not represented.

2.3.3. Local atomic volume. The local atomic volume of an atom corresponds to the space closer to this atom than to any other atom. It thus characterizes the real space an atom has. This local atomic volume was computed according to the methodology described by Domain and Becquart [14].

2.3.4. Coordination. In this work, the coordination is defined as the number of Fe atoms within a 2.3 Å radius sphere around the C atom. In an iron bcc lattice (lattice parameter at 0 K predicted by the EAM potential used throughout this work $a_0 = 2.855\,32$ Å), interstitial C atoms position themselves in octahedral sites rather than tetrahedral sites [30]. In pure iron, in an O site, the coordination is 6; there are two iron atoms at $\frac{a_0}{2} = 1.43$ Å and four iron atoms at $\frac{\sqrt{(2)}a_0}{2} = 2.02$ Å. The third closest neighbours of the C atom are eight iron atoms at $\frac{\sqrt{(5)}a_0}{2} = 3.19$ Å. According to the interatomic potential we use in this work, when a C atom is introduced in the O site and the structure is relaxed, the two Fe 1st nearest neighbours move away from the C atom from 1.43 Å to 1.79 Å whereas the four Fe 2nd nearest neighbours move closer to the C atom from 2.01 Å to 1.98 Å. Therefore, a coordination non-equal to 6 would mean a distorted lattice around the C atom because it would mean that an Fe atom moved by at least 0.3 Å.

2.4. Dynamic calculations: kinetic-ART

Contrary to standard AKMC methods, kinetic-ART (k-ART) is an off-lattice/self-learning AKMC, i.e. that it does not constraint atomic positions to a rigid lattice, and an event catalogue is constructed on-the-fly by the program as the simulation proceeds. It makes this technique especially suitable for the study of activated diffusion processes [31, 32] such as carbon diffusion in Fe [26] and reproduce the lattice even in distorted systems. K-ART identifies all the possible transitions for each local topology, defined by the graph composed of the links between the different atoms. For a given system, with a

specific potential, there is a bijection between the topology and the real lattice. Another important assumption made is that for a given topology, the possible transitions will remain the same. This means that for a topology, the transitions have to be computed only once. The relevant energy barriers, i.e. those with an occurrence probability of 0.01% or more, are recalculated at each step to ensure that the transitions, even if they are the same, have the right energy. This implies that k-ART, unlike more standard KMCs include exactly the effect of elastic deformations on minima and barriers, allowing one to study the diffusion of carbon near a dislocation core. The topologies of the system are managed by NAUTY [33]. K-ART uses a local transition searching method which finds all the jumps associated with a given system and their associated energies [34]. The method works by directly computing the lowest curvature using the iterative Lanczos algorithm, an efficient method allowing to follow a local eigendirection [35]. From a configuration in a local minimum, the program will find all the associated transitions barrier as well as the local minimum after the jump. Contrary to other saddle point searching methods such as the nudged elastic band method, only one local minimum is needed to find a transition barrier.

The simulations were launched in order to study the impact of the addition of C atom(s) near the i19 dislocation loop. Therefore, we introduced an i19 loop in a perfect Fe matrix with one or two C atoms. For all k-ART simulations, the temperature was set to 300 K or 600 K in a $9 \times 9 \times 9$ bcc supercell.

3. Results

3.1. Static properties

Figure 2 represents the C $-$ ½ ⟨1 1 1⟩ loop binding energy for the DFT calculations as well as the empirical potential, and for the two investigated box sizes (the 1458 atomic volume box and the $1458 + 19$ atomic volume box). The binding energy is defined so that the most stable configurations are the ones with the highest binding energy (section 2.3.1).

Regarding the influence of the box volume on its energy, one could expect that it would only cause a shift in the simulation box energy (hence in the binding energy) equal to the constraint added by the 19 SIAs. However, figure 2 indicates that the addition of 19 atomic volumes to the simulation box volume does not induce a strict shift in the binding energy. This can be due to the fact that the lattice does not relax in the exact same configuration when the relaxation is done in the two different boxes or that deformations are sufficiently important to sample non-linear parts of the interaction. As seen on figure 2, the difference in binding energies between configurations relaxed by DFT with and without the addition of 19 atomic volumes is higher than the difference in binding energies between configurations relaxed by EP with and without the addition of 19 atomic volumes. Therefore, it is possible to deduce that DFT is more sensitive to the change of pressure than the empirical potential.

We can observe on figure 2 that the most stable configurations for the C atom are the ones at the external periphery

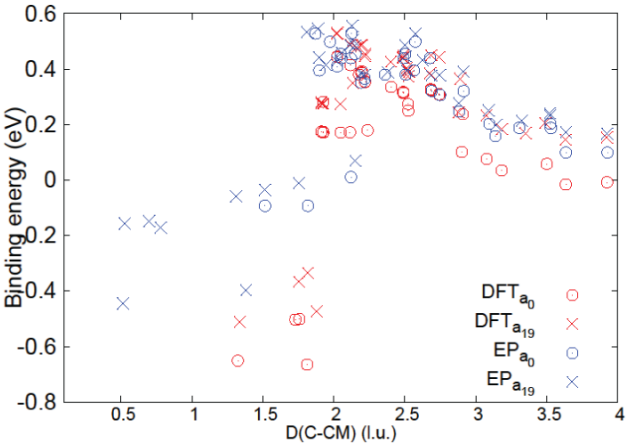

Figure 2. Binding energy between the C atom and the ⟨1 1 1⟩ loop (DFT and empirical potential calculations labelled as DFT and EP) versus D(C-CM) for lattice parameter taking and not taking into account the loop pressure induced dilatation (labelled as a_{19} and a_0 respectively). The results are presented for simulations containing a loop and a C atom as only defects in a $9 \times 9 \times 9$ bcc Fe matrix.

of the loop (D(C-CM) $>$ 2 lattice unit (l.u.)), with a binding energy of 0.44 eV (resp. 0.50 eV) for the DFT (resp. for the empirical potential) calculations in the 1458 atomic volume box. The covalent Fe–C interaction potential derived by Hepburn [36] predicts binding energies of the same order. Note, however, that the Hepburn potential has been found to disagree with DFT calculations regarding the carbon-dislocation interaction. Indeed, as highlighted by Terentyev *et al* [7], the saddle point predicted by this potential as the C atom migrate is not the tetrahedral site, whereas the potential used in this work [15, 23] agrees qualitatively with the DFT calculations regarding the attractive carbon dislocation interaction of about 0.1 and 0.4 eV for carbon–carbon separations of 1*b* and 2*b* respectively [37]. Using a combination of an Fe potential developed by Ackland [38] and an FeC potential developed by Johnson [39], Tapasa *et al* [9] observe that the binding energy of C with small ⟨1 1 1⟩ loops decreases with the loop size from 0.86 eV for a four SIA loop to 0.42 eV for a 19 SIA loop, close to the value of 0.55 eV predicted by the potential used in this work for the binding energy between C and a 19 SIA loop. The strength of the C-loop interaction predicted by the empirical potential used through this work is in between that of the highest binding energy of C atom in a screw dislocation core (0.41 eV) and the highest binding energy of a C atom in an edge dislocation core (0.65 eV) [24] obtained with the same potential before the slight adjustment done by Veiga [23].

Even if the binding energies predicted by the DFT and the empirical potential are not strictly the same especially for repulsive configurations, there is an excellent agreement in the trend of the curves figure 1 thus confirming that the empirical potential is in good agreement with the DFT calculations. One can furthermore observe on figure 2 that for the same D(C-CM) different binding energies can be obtained. The main reason for this behaviour is due to the fact that the dumbbells constituting the loops have low migration barriers along the ⟨1 1 1⟩ direction; these can then move easily, therefore the energy of

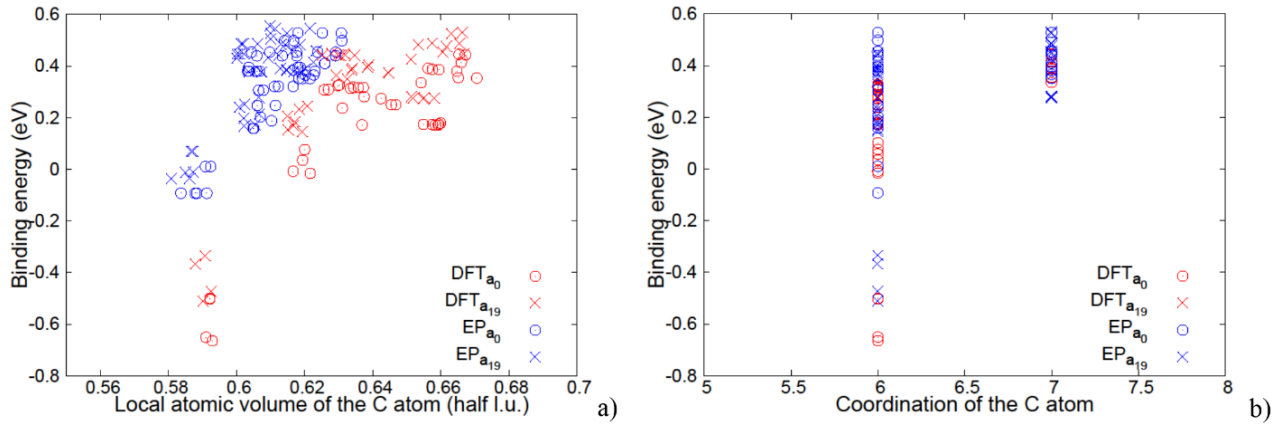

Figure 3. C-⟨1 1 1⟩ loop binding energies (DFT and empirical potential calculations) versus (a) the local atomic volume (b) the coordination number for lattice parameter taking and not taking into account the loop pressure induced dilatation. The results are presented for simulations containing a loop and a C atom as only defects in a $9 \times 9 \times 9$ bcc Fe matrix.

the box changes and so does the binding energy between the C and the loop. Despite this issue, figure 2 provides a good overview of the system: for a C-loop centre of mass distance under 1.9 l.u., all the binding energies are repulsive meaning that the loop and the C atom are likely to go far away from each other. Conversely, the most attractive configurations are the ones with the C atom at the external periphery of the loop (2–2.2 l.u.). Finally, one can observe that the empirical potential tends to underestimate the repulsion between the defects compared to DFT.

A correlation between the local atomic volume and the binding energy is emerging from figure 3(a): the more space a C atom has, the more attractive the interaction energy between the two defects. All configurations where the local atomic volume of the C atom is below 0.6 are repulsive. One can deduce from figures 2 and 3(a) that the most spacious configurations for the C atom are the ones where C is at the external periphery of the loop. Conversely, that the most stable configurations are the ones where the C atom is at the external boundary of the loop because this is where the carbon has the most space thus disturbing the less the iron matrix. Figure 3(a) also points out that the potential predicts smaller atomic volumes than DFT.

Figure 3(b) provides interesting information: the highest binding energies are obtained when the C atoms have seven Fe atoms closer than 2.3 Å to them. These configurations share a particular characteristic: the C atom is 2.3 Å close to only one or two atoms of the loop which corresponds to the carbon atom being at the external boundary of this loop. Inside the loop, the coordination is 6, which confirms that inside the loop the organization of Fe atoms is the same as for the bcc iron matrix. The surprising result is that the C atom is strongly bound to the loop when there are 7 Fe atoms close to it, so more than the C atom in pure iron. Strong binding energies also correspond to the largest local atomic volumes leading to the counter-intuitive fact that the more iron atoms in a 2.3 Å sphere around the C atom the larger the space around the C atom. A plot of the local atomic volume versus the coordination confirms that the C atoms having a coordination of 7 do have a high local atomic volume thus a strong binding energy between the defects.

Figure 4 summarizes the binding energy datasets obtained in this work. The main difference on these datasets is the change in the repulsive binding energies: on figure 4(a), (b) and (d), the most repulsive configurations have a binding energy below −0.4 eV when on figure 4(c) the most repulsive configurations have a binding energy close to −0.1 eV. This is due to the differences in configurations, because for the empirical potential relaxation without the 19 atomic volumes, no C atom was found far within the loop after the relaxation and the closer the C atom to the loop centre of mass the greater the repulsion.

To summarize, one can observe in figure 5 that the most attractive configurations are the ones where the carbon is at the external boundary of the loop and close to the plane (1 1 1) containing the loop centre of mass. The sudden drop of the surface occurs at the loop boundary, confirming that the binding energy becomes repulsive when the C atom enters the loop.

A closer look at the binding energies of all the configurations leads us to sort the configurations in three sets of binding energies. Because no configuration relaxed by EP with the addition of 19 atomic volumes was found to have a binding energy between 0 eV and 0.069 eV and between 0.28 eV and 0.37 eV, we decided to classify the configurations depending on their binding energy into three distinct categories, namely high binding energies category (Eb $>$ 0.3 eV), low binding energy category (0 eV $<$ Eb $<$ 0.3 eV) and repulsive category (Eb $<$ 0 eV). We thus expect to find the same kinetic behaviour for configurations in the same category.

Figure 6 summaries these three categories of initial configurations depending on the C position with respect to the loop: high binding energy configurations when the C is at the external periphery of the loop in green, low binding energy configurations when the C is far from the loop in red and repulsive configurations when the C is within the loop in blue (this colour code will be used throughout the whole paper). A precision must be added to the repulsive category, because the configurations with a repulsive binding energies close to 0 eV (−0.01 eV and −0.03 eV) are the ones where the C atom is not directly within the loop and not even in the plane comprising

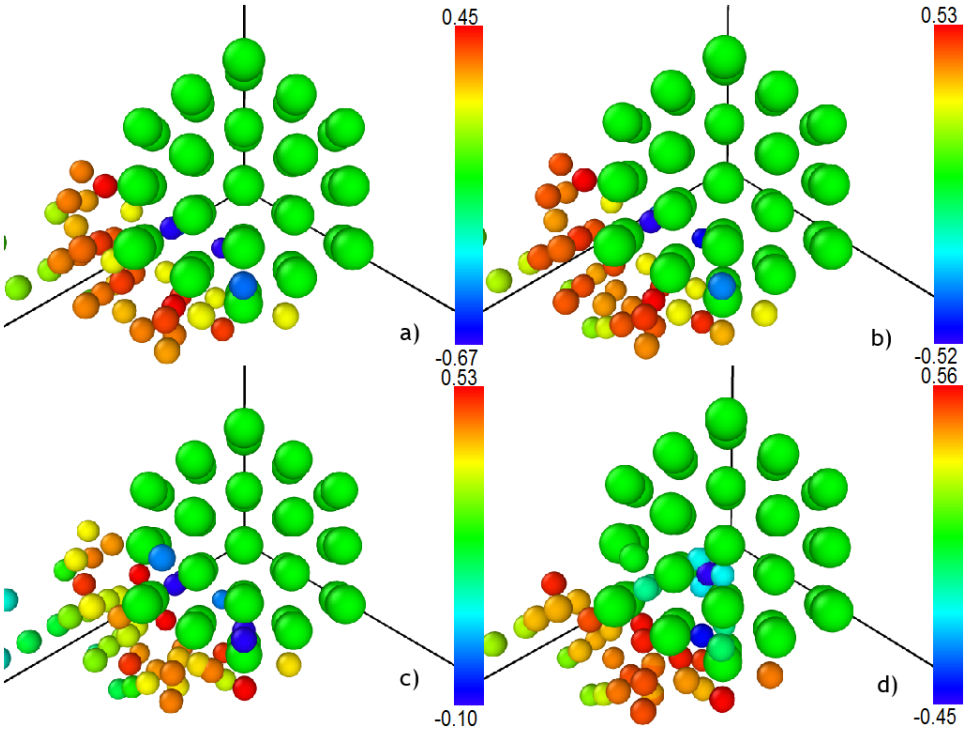

Figure 4. Binding energies in eV between the C atom (small colourized atoms) and the loop (large green atoms) for different configurations using the different relaxation techniques presented: (a) DFT without 19 atomic volumes added, (b) DFT with 19 atomic volumes added, (c) empirical potential without 19 atomic volumes added, (d) empirical potential with 19 atomic volumes added. The C atoms are colourized according to their binding energy with the loop. The perfect loop is showed for comprehension sake because the loop shape is different for each initial configuration.

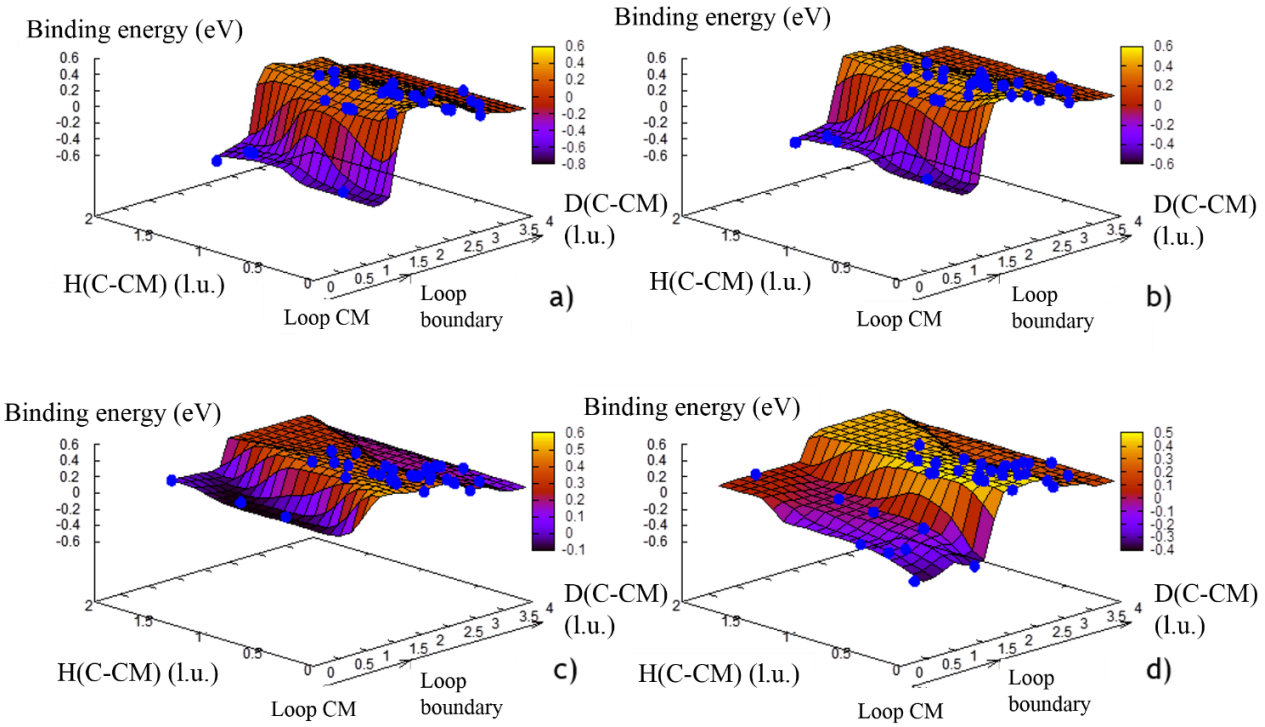

Figure 5. Binding energy surfaces constructed with the binding energy of initial configurations of simulations containing a loop and a C atom as only defects in a $9 \times 9 \times 9$ bcc Fe matrix (blue dots). The results for the different relaxation techniques are presented: (a) DFT without 19 atomic volumes added, (b) DFT with 19 atomic volumes added, (c) empirical potential without 19 atomic volumes added, d) empirical potential with 19 atomic volumes added. The *x* axis is D(C-CM) and the *y* axis is H(C-CM). The surface's colour refers to the Eb colour code.

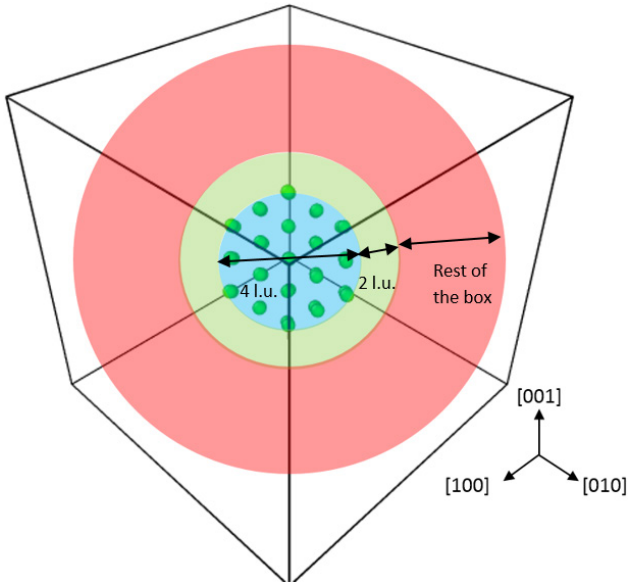

Figure 6. Classification of initial configurations depending on the C position. The green atoms represent the perfect loop for simplification sake. For C atoms in the blue zone, the configuration is repulsive (Eb $<$ 0 eV); for C atoms in the red zone, the configuration is in the low binding energy category (0 eV $<$ Eb $<$ 0.3 eV); for C atoms in the green zone, the configuration is in the high binding energy category (Eb $>$ 0.3 eV).

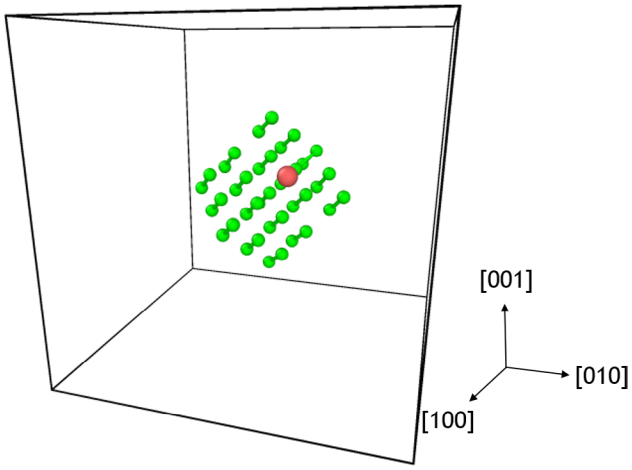

Figure 7. Configuration relaxed by the empirical potential with a binding energy, Eb $= -0.13$ eV indicating a repulsion between the C (red atom) and the loop (green atoms) even if the C atom is not on the same $\langle 1\,1\,1 \rangle$ plane as the loop. This system contains a loop and a C atom as only defects in a $9 \times 9 \times 9$ bcc Fe matrix (not represented for simplification sake).

the loop (e.g. figure 7). These configurations are thus the ones where H(C-CM) is high and D(C-CM) is lower than 2 l.u. Still, a repulsive energy between these defects suggests that the loop will likely go away from the C atom. This result may be easily explained by the fact that if the loop goes towards the C atom until the C is within the loop, the resulting configuration will be less stable than the original configuration, i.e. the configuration has a lower energy when the C atom is above the loop than the one where the C atom is within the loop.

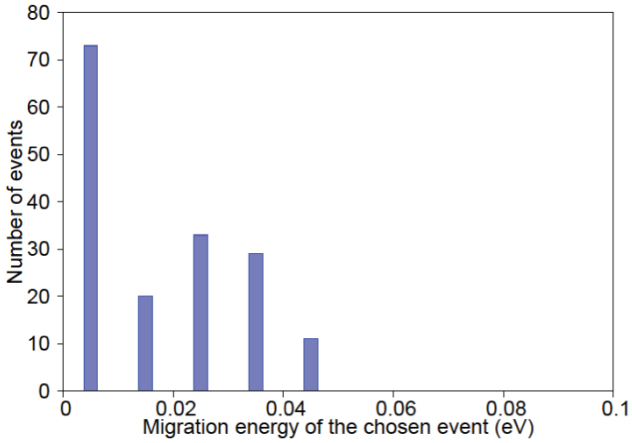

Figure 8. Migration energy of the events chosen by the KMC for a 176 step simulation containing the i19 loop as only defect in a $9 \times 9 \times 9$ bcc Fe matrix.

3.1.1. K-ART simulations. In order to have a good overview of all the simulations, a summary of each MD and KMC simulation is given in the table 'Summary of all simulations' in supplementary material (stacks.iop.org/JPhysCM/30/335901/mmedia).

3.1.1.1.Loop mobility in a pure Fe matrix. In pure iron, the i19 loop is known to be a very mobile defect. A simulation was launched with an i19 dislocation loop as only defect in a pure Fe matrix in a $9 \times 9 \times 9$ box at 300 K to confirm that result. The highest energy barrier found in a 176 step simulation is approximatively 0.05 eV for a crowdion to move as seen on figure 8.

Even if not a single crowdion was found far from the others, meaning that the loop will move as fast as its slowest crowdion, the energy barriers are so low that the overall mobility of the loop is enormous. For this simulation, the timestep of the different events were found to be between 10^{-13} s and 10^{-16} s.

3.1.1.2.Loop interaction with one C atom. We have run 40 k-ART simulations for an average computing time of 2.5×10^5 s at 300 K starting on the configurations relaxed by empirical potential with the addition of 19 atomic volumes, so for $9 \times 9 \times 9$ bcc Fe boxes with a C atom and an i19 loop. One first important result is that the average time step for a C jump is approximatively 10^7 times higher than the average time step for a crowdion displacement. The loop moves thus a lot faster than the C atom and the difference in the defect velocities suggests that the dislocation loop will move until it encounters a C atom.

The energy needed for the C atom to jump in the first step of all the simulations with 1 C atom at 300 K is presented figure 9. The simulations are divided in the three categories defined in 3.1. Knowing that the C migration energy predicted by our potential in a perfect Fe lattice is 0.815 eV, one can deduce from figure 9 that the loop has a high influence on the mobility of the C atom. When the C atom is initially inside the loop (repulsive category), the C migration energies are lower than the C migration energy in a perfect Fe bcc lattice

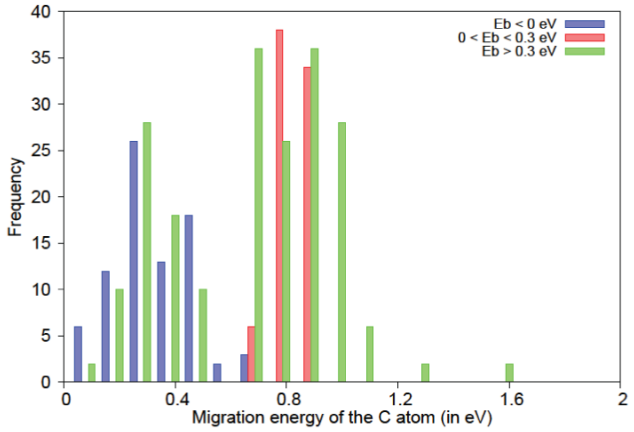

Figure 9. C migration energy for different initial configuration binding energy categories at the first step of the simulation: high binding energies category (Eb $>$ 0.3 eV), low binding energies category (0 eV $<$ Eb $<$ 0.3 eV) and repulsive category (Eb $<$ 0 eV). The simulation boxes contain a loop and a C atom as only defects in a $9 \times 9 \times 9$ bcc Fe matrix.

($E_{mig} < 0.8$ eV). This reflects that the loop will be likely to unpin from this C atom. For initial low binding energy configurations, the C jump energy is close to the migration energy of C in a perfect bcc lattice. From these configurations where the C atom is far from the loop, one can deduce that the interaction between the two defects is weak. More interestingly, for initial high binding energy configurations, two main areas divide the carbon migration energy. On the one hand, it was logically found that the C atom strongly linked to the loop has a close to or a higher jump energy than 0.8 eV. On the other hand, a lot of C migration energies are below that threshold of 0.8 eV, leading to the counter-intuitive idea that the C atom may move easily. A possible explanation linked to this observation is that a zone of stability around the loop exists thus allowing the C atom to move almost freely around the loop and staying in a strong binding position with it.

Representative simulations of the three categories are represented in figure 10(a) (for the high binding energy configurations), figure 10(b) (for the low binding energy configurations) and figure 10(c) (for the repulsive configurations). These representative simulations represent all the behaviours observed for the three categories of initial configurations with a loop and 1 C atom at 300 K.

As seen on figure 10(a), when the initial binding energy is high, the C-CM distance does not change much meaning that the loop does not move away from the C atom. For all these simulations, we never observed the loop leave the C atom. Even if in a few of these simulations the loop tends to go away from the C atom, it never really leaves it, e.g. when only one crowdion of the loop is close to the C atom while the others are far. This shows the pinning power the C atom has on the loop: strongly bound to a crowdion and because the cohesive force of the loop prevents its break-up, it is hard for the loop to move in these particular conditions.

Figure 10(b) represents the two different behaviours observed for initial low binding energy configurations (0 eV $<$ Eb $<$ 0.3 eV). The first one (solid line) shows the ability of the loop to go away from the C atom when the two

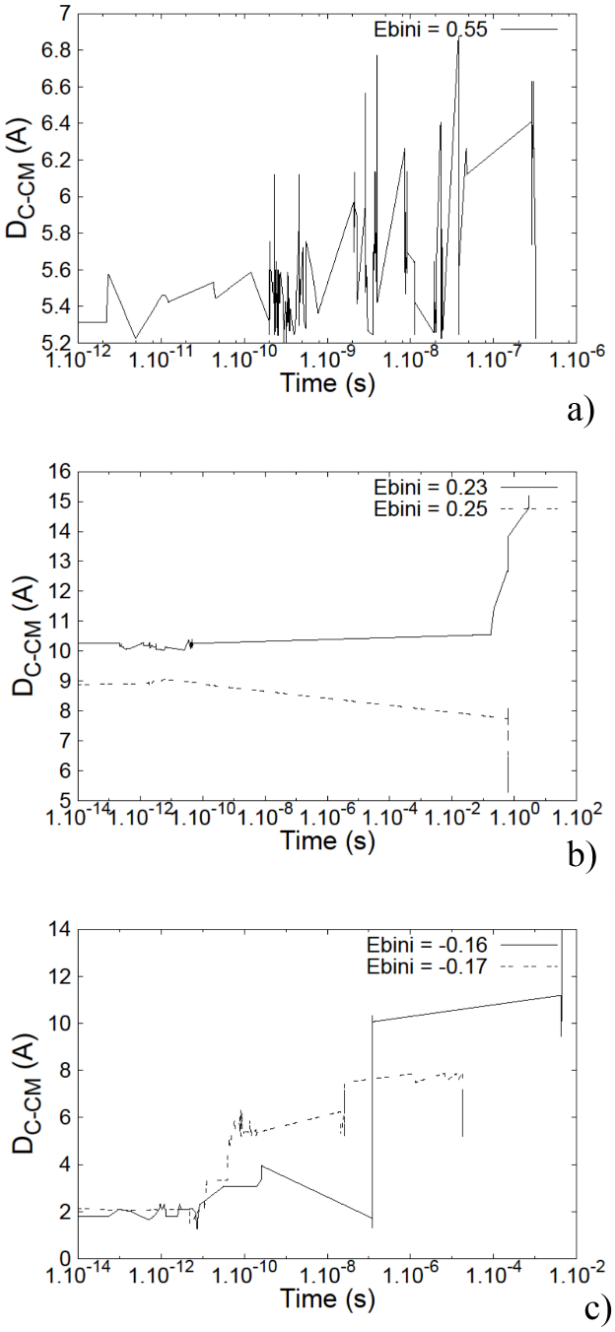

Figure 10. Evolution of the distance between the C atom and the loop centre of mass for representative simulations of the different categories of initial configurations: initial high binding energy configurations (a), initial low binding energy configurations (b) and initial repulsive configurations (c). The simulations contain a loop and a C atom as only defects in a $9 \times 9 \times 9$ bcc Fe matrix.

defects are not so close i.e. the interaction is low. On the contrary, the second one (dashed line) shows the ability of the C atom to move towards a more stable position, so towards the loop external periphery. Therefore, there is a competition between the C atom weakly pinning the loop and the loop movement. One can think that among the low binding energy configurations, the ones with the highest binding energy will lead to the migration of the C atom to the external periphery of the loop and the ones with the lowest binding energy will lead to the migration of the loop, but in fact it was found that even

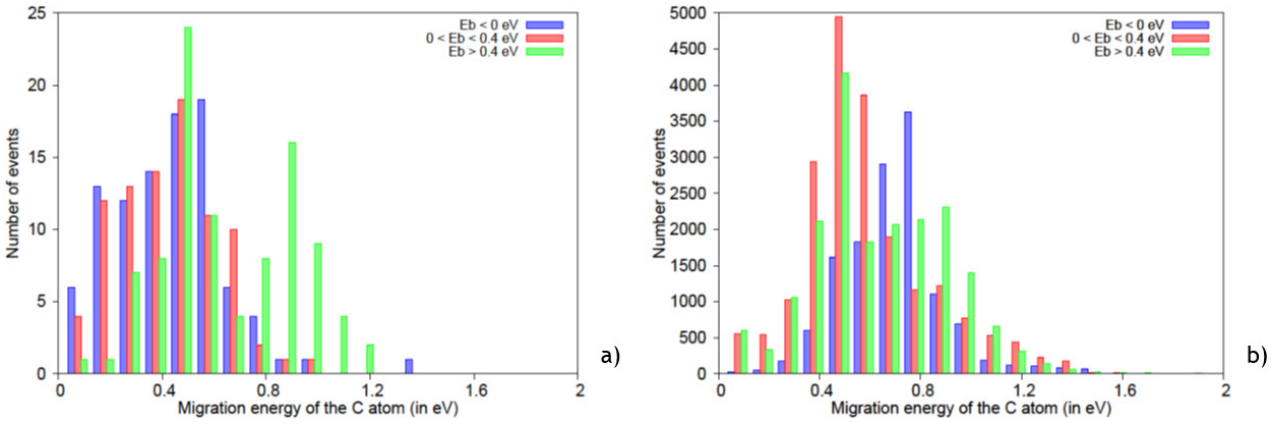

Figure 11. C migration energy for different initial configurations with two C atoms and a loop for the first step (a) and for the whole simulation (b). The initial configurations are divided into three categories: high binding energy (Eb $>$ 0.4 eV), low binding energy (0 $<$ Eb $<$ 0.4 eV) and repulsive (Eb $<$ 0 eV). The simulation boxes contain a loop and two C atoms as only defects in a 9 $\times$ 9 $\times$ 9 bcc Fe matrix.

with binding energies of 0.17 eV the C atom can be found at the external periphery of loop and that the highest binding energy configuration (0.28 eV) lead to the loop moving with no movement of the C atom. This proves the stochastic character of this effect. This competition is found in two simulations, namely the ones with a binding energy 0.17 eV and 0.20 eV, in which the two effects are occurring at the same time: the loop moves a little away from the C atom but the C will still come to a strong binding position; at the end of these simulations, both defects have moved from their original places thus showing a weak enough anchoring of the loop for it to move but also a strong enough interaction between C and the loop for the C to migrate.

Figure 10(c) represents the two typical evolutions of the C-loop system found for initial repulsive configurations, namely the drive-away process of the loop from the C atom and the repositioning of the C atom to the most stable configurations. The first one (solid line) is simple to explain: the loop will move away from the C atom hindering the stability of the system. The simulation of the second behaviour (dashed line) shows a jump by jump migration of the C atom from within the loop through its external periphery. As shown in figure 9, the C migration energy within the loop is lower than the C migration energy in a perfect Fe lattice, suggesting a low energy migration pathway of the C atom to the external periphery of the loop. Once again, a competition occurs between the loop wanting to move and the C atom wanting to migrate to the most stable configurations. But for the C to migrate, the loop must be anchored a minimum. Therefore, even a C atom within the loop has a pinning effect on the loop although the two defects have a repulsive interaction.

To conclude on this first set of results at 300 K, only two different endings were found to all these simulations. Either the C atom is found at the external periphery of the loop, to the strongest pinning positions, or the pinning was not sufficient enough and the loop was found far from the C atom.

3.1.1.3. Loop interaction with two C atoms. We now investigate the impact of two C atoms on the mobility of the dislocation loop by launching 20 k-ART simulations at 300 K in 9 $\times$ 9 $\times$ 9 bcc Fe supercells with two C atoms and the i19 loop. Considering that there are three different categories for one C atom (see figure 6), six different combinations of initial configurations are possible for two C atoms simulations. However, as seen on figure 9, for initial low binding energy configurations where the C atom is far from the loop, the influence of the loop on the C migration energies is weak. We thus decided to focus our attention on simulations with C atoms in repulsive positions or in high binding energy positions. Therefore, only three different categories of initial configurations are possible: two C atoms within the loop, two C atoms at the external periphery of the loop and one C atom within the loop with one C atom at the external periphery of the loop. Looking at all the different initial configuration binding energies with two C atoms, we classify the configurations in three categories: repulsive category (Eb $<$ 0 eV, two C atoms within the loop), low binding energy category (0 $<$ Eb $<$ 0.4 eV, one C atom within the loop and one C atom at the external periphery of the loop) and high binding energy category (Eb $>$ 0.4 eV, two C atoms at the external periphery of the loop). The choice for these categories is, again, justified by the gap in the binding energies of the configurations: no configurations are found with an Eb between $-$0.36 eV and 0 eV and neither between 0.35 eV and 0.56 eV.

Figure 11 puts on display the migration energy of the C atom for all the simulations with two C atoms for the first step (a) and for all the steps (b). Doing the comparison between the initial C migration energy for configurations with one C atom (figure 9) and two C atoms (figure 11(a)) leads to the following observations.

– For initial high binding energy configurations, there are still the two distinct sets of migration energies, i.e. the low migration energy set ($E_{\mathrm{mig}} < 0.8$ eV) and the high migration energy set ($E_{\mathrm{mig}} \geqslant 0.8$ eV) meaning that the zone of stability of the C atom around the loop still exists.
– For initial repulsive configurations, whether one or two C atoms are within the loop, almost all the migration energies are low ($E_{\mathrm{mig}} < 0.8$ eV) suggesting that the C atom and the loop are still likely to move away from each other.

– For initial low binding energy configurations, a difference in the C migration energies is observed whether the box contains one C atom or two C atoms. Indeed, when there is only one C atom (figure 9), C migration energies are close to C migration energy in a perfect bcc lattice ($E_{mig0} = 0.815\,eV$) whereas when there are two C atoms, C migration energies are mostly low ($E_{mig} < 0.8\,eV$). Remember that this is due to the differences in configurations: for the configurations in the initial low binding energy category with two C atoms, one C atom is in a strong attractive position and one C atom is in a repulsive position. Therefore, one should expect to observe low C migration energies due to the C atom in a repulsive position as well as both high and low C migration energies due to the C atom in a high binding energy position (as seen on figure 9). However, very few high energy barriers were found for the initial low binding energy configurations in figure 11. This means that the interaction between the two C atoms helps the C atom in a strong binding position to overcome the high energy barriers. The consequence of the interaction between the C atoms is then a lowering of the high energy barriers.

The evolution of the C-CM distance for the three categories of initial configurations with two C atoms is represented on figure 12. For the simulation initially in the high binding energies category so with two C at the external periphery of the loop (figure 12(a)), one can observe that the C-CM distance between the interstitials and the loop centre of mass did not evolve much. In fact, as seen on figure 13, the C atoms simply moved in the stability zone around the loop. An interesting phenomenon occurred in one of the simulations in the high binding energies category: the loop moved during the simulation while dragging the C atoms with it as seen in figure 14 through very-low migration energy transitions (around the meV). All the simulations in the high binding energies category were found to have the same ending, i.e. the two C atoms were situated in strong attractive positions at the end of the simulations.

For initial low binding energies configurations (with one C atom in a strong binding position and another one within the loop), two different endings of the simulations were reached. On the first scenario, the loop moves away rapidly from the C atoms because one C atom is within the loop. On the second scenario presented on figure 12(b) and illustrated on figure 15, the C atom within the loop moves as far as the loop periphery thus becoming strongly bound with the loop. Instead of having one C within the loop and only one anchoring point as the C atom at the external periphery like at the beginning of the simulation, there are now two strong anchoring points for the loop: the initial low binding energy configuration figure 15(a) became an initial high binding energy configuration figure 15(b) and just like other simulations of this category, the two C atoms moved freely around the loop (figure 15(c)). However, if the outcomes of the simulations in the low binding energies category are different, they share a particular detail: the C atom within the loop never moved towards the loop centre. This behaviour can be easily explained because

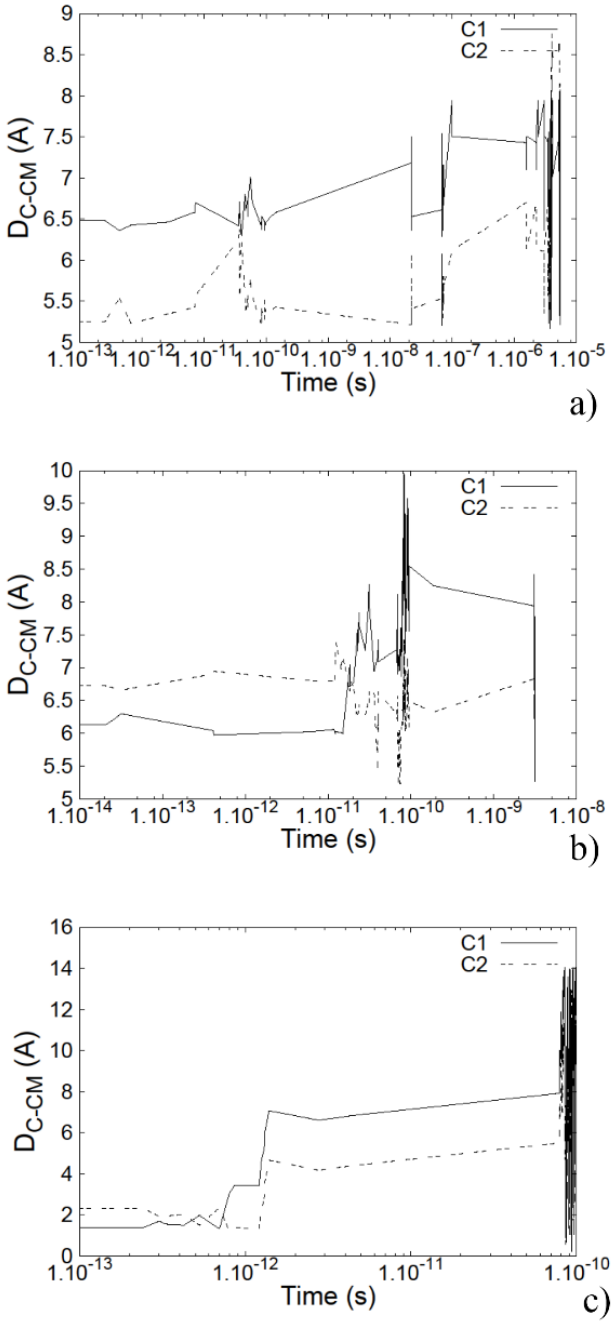

Figure 12. Evolution of the distance between the loop CM and the C atoms for k-ART simulations at 300 K with two C atoms representative of the three binding energy categories: high binding energies category (Eb = 0.91 eV (a)), low binding energies category (Eb = 0.23 eV (b)) and repulsive category (Eb = −1.29 eV (c)). The simulation boxes contain a loop and two C atoms as only defects in a $9 \times 9 \times 9$ bcc Fe matrix.

the closer the C atom to the loop centre of mass, the higher the total energy and so the lower the stability of the system.

The addition of another C atom tends to enhance all the phenomena occurring with one C atom, whether it is the loop unpinning from a C atom within it or the free movement of C interstitials around the loop. It can be easily explained for the first case because two repulsive forces will make the loop move faster. As for the second case, adding a C atom

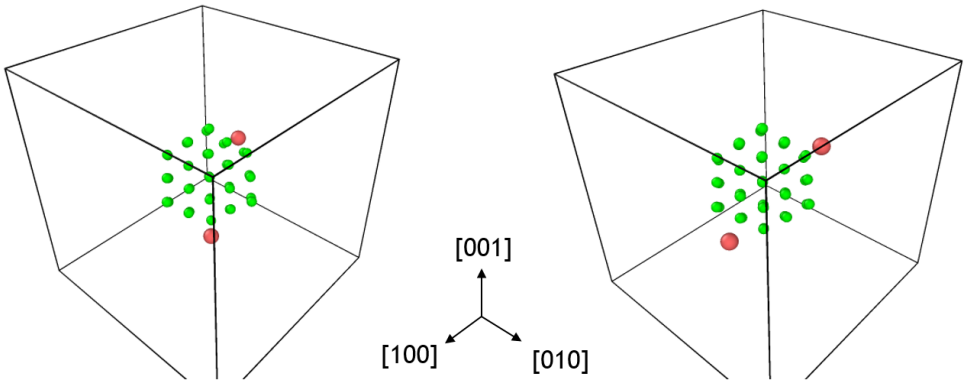

Figure 13. Initial (left) and final (right) configurations exhibiting the movement of the C atoms (red atoms) around the loop (green atoms) for a simulation with 2 C atoms bound to the loop at the beginning (Eb = 0.91 eV). The simulation contains a loop and two C atoms as only defects in a 9 × 9 × 9 bcc Fe matrix (not represented for simplification sake).

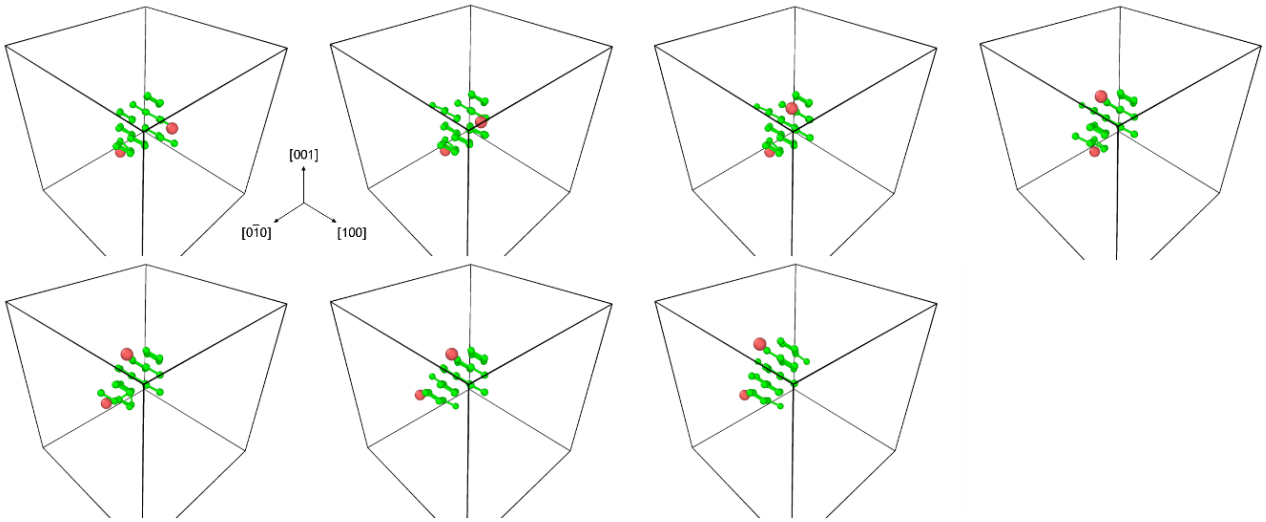

Figure 14. Snapshots of a k-ART simulation exhibiting the dragging effect of the loop (green atoms) which stays close to the C atoms (red atoms) when moving for a simulation with two C atoms bound to the loop at the beginning (Eb = 0.91 eV). The different snapshots were taken in a range of 20 steps with activation energies around 1 meV (steps with very low movements were skipped). Each step represents a simulated time between 10^{-15} s and 10^{-11} s. The box contains a loop and two C atoms as only defects in a 9 × 9 × 9 bcc Fe matrix (not represented for simplification sake).

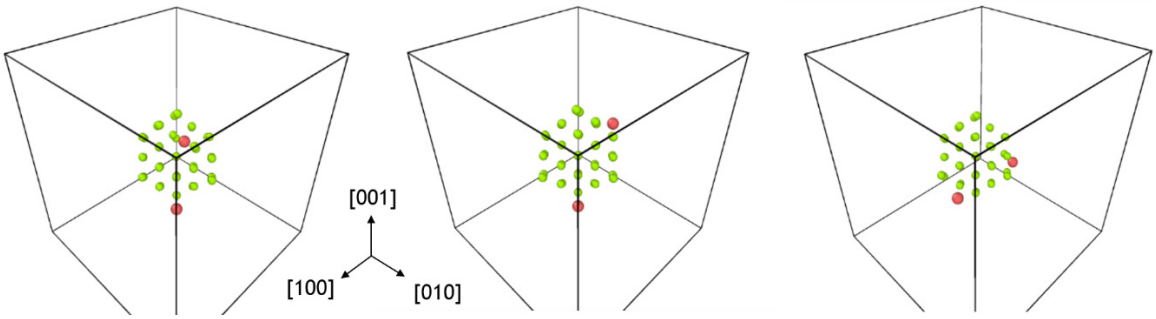

Figure 15. Representation of the evolution of a system with two C atoms (red atoms) and loop (green atoms) for an initial low binding energy configuration where 1 C is at the external periphery of the loop and the other one is within the loop (a). The snapshot (b) represents the moment the C atom within the loop went at the external periphery and (c) represents the end of the simulation. The simulation contains a loop and 2 C atoms as only defects in a 9 × 9 × 9 bcc Fe matrix (not represented for simplification sake).

provides another anchoring point allowing the other C atom to move freely.

It seems obvious that two C atoms can pin the dislocation loop more efficiently than a single C atom because the second C atom provides an additional anchoring point; higher energy is therefore needed for the loop to unpin. Furthermore, just as in the case of the double kink mechanism [40], the whole loop can be dragged by the displacement of a single crowdion, therefore locking down two crowdions instead of one will result in lower chances for the loop to provide mobile crowdions which

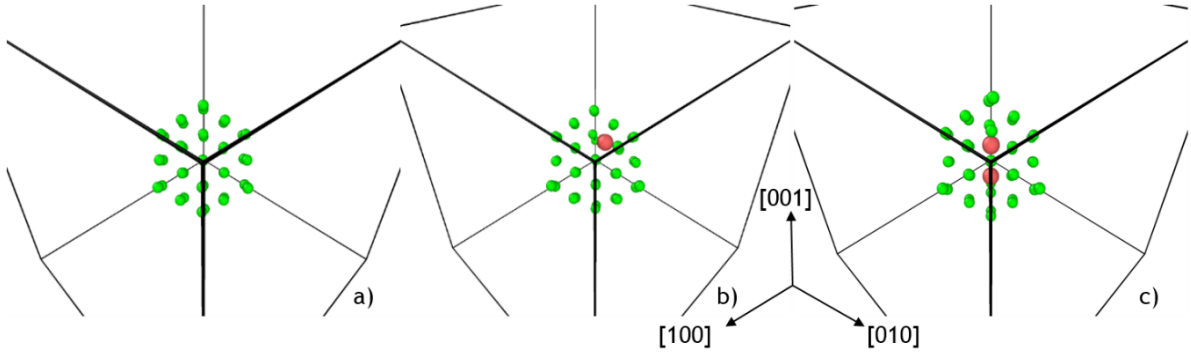

Figure 16. Loop distortion effect induced by the presence of two C atoms (red atoms) within the loop (green atoms), Eb $= -0.60$ eV (b) and Eb $= -1.29$ eV (c) comparing with the loop alone (a). The simulation contains a loop and two C atoms (only for (b)) and (c)) as only defects in a $9 \times 9 \times 9$ bcc Fe matrix (not represented for simplification sake).

can drag the whole loop. However, no simulation with two C atoms has a simulated time higher than 10^{-4} s at 300 K so it is impossible to compare it with the simulations with one C atom. The main reason for that difference in the simulated time is linked to the presence of the second C atom. As this atom adds more possible transition at each step, with more low energy barriers (mainly between 0.2 and 0.5 eV, figure 11(b), the effective transition rate increases thus lowering drastically the time step. As seen previously, the great increase of the time step is due to a strong pinning of the loop removing the loop crowdions very-low barrier transitions thus leaving the C atom the only mobile defect. So adding another mobile C atom in this configuration results in a lower time step.

3.2. Influence of temperature

The temperature was then set at 600 K to investigate the effect of temperature. The main effect we observed is the enhanced mobility of the loop. Even in the simulations done with two C atoms, at this temperature, very few movements of the C atoms were found. The main drawback of this observation is the difficulty to interpret the results given by the simulations. Indeed, very-low migration energy events (flickers) lead to a significant decrease in the time step of KMCs and so on the simulated time. Fortunately, the simulated time of these simulations is reachable by molecular dynamics. Therefore, the effect of the temperature will be discussed only on MD simulations.

3.3. MD simulations

Simulations matching the KMC conditions were launched by MD, so with one and two C atoms, at 300 K and 600 K in a $9 \times 9 \times 9$ box. For these simulations, the timestep is set to 1 fs in the NVE ensemble for a total simulated time of 100 ns. The same trends were found with both methods, even if some differences are observable: the C atoms still want to move towards the external periphery of the loop, the loop can be pinned by C atoms and when it is done, the C atoms can freely move around the loop. The main difference between KMC and MD simulation is the fact that for every simulation in the low binding energies category launched by MD with one C atom, the competition between the loop wanting to move and the C atom wanting to go towards the loop periphery does not appear anymore. Indeed, at 300 K and even at 600 K, the C atom was never found to move to the external periphery of the loop, and while it can move a little, the loop rapidly goes away from it.

For all the simulations in the repulsive category launched (two C within the loop), at 300 K and 600 K, done by MD and KMC, the loop promptly goes away from the C atoms. Comparing this result with the simulations in the repulsive category with one C atom leads to the conclusion that even if the C atoms are pushed towards the loop external periphery, as proved by figures 11(a) and (b) where the migration energies of the C atoms are mostly lower than the migration energy of the C atom in a perfect Fe lattice, the repulsion between the loop and the two C atoms is too high for the loop to wait for the migration of the C atoms and so it rapidly moves away from the interstitials. The reason why the loop moves promptly can be explained by the high distortion of the loop induced by the presence of the two C atoms inside, even going as far as changing the crowdions alignment as seen on figure 16. The only possibility for the system to be stable again is the displacement of the loop. To prove the strength of this effect, even for an initial configuration with two C atoms very close (Eb $= -0.6$ eV), thus repelling each other, we observe that the loop moves first away from the C atoms, and then the two C atoms move away from each other. In only a very few number of simulations did we observe one of the C to jump before the loop went away, but the C atom never reached the loop external periphery. To conclude, the addition of a second C atom within the loop distorts the loop so much that it cannot stay close to the C atoms. They may rearrange but only after the loop has moved away.

Finally, the MD simulations with two C atoms were launched again but in a larger box, i.e. a $20 \times 20 \times 20$ box (16 000 lattice Fe atoms, 19 SIA loop atoms and two C atoms) in order to check the impact of using small boxes and in particular interaction with the periodic images. An interesting phenomenon was observed for initial repulsive configurations. For all these simulations, at 300 K and 600 K, the loop rapidly moves away from the C atoms. However, when the loop comes back towards the C atoms because of the periodic boundary conditions, it moves back almost all of the time without crossing over the C atoms: the C atoms do not return back within the loop and so the loop is trapped in a back and forth movement

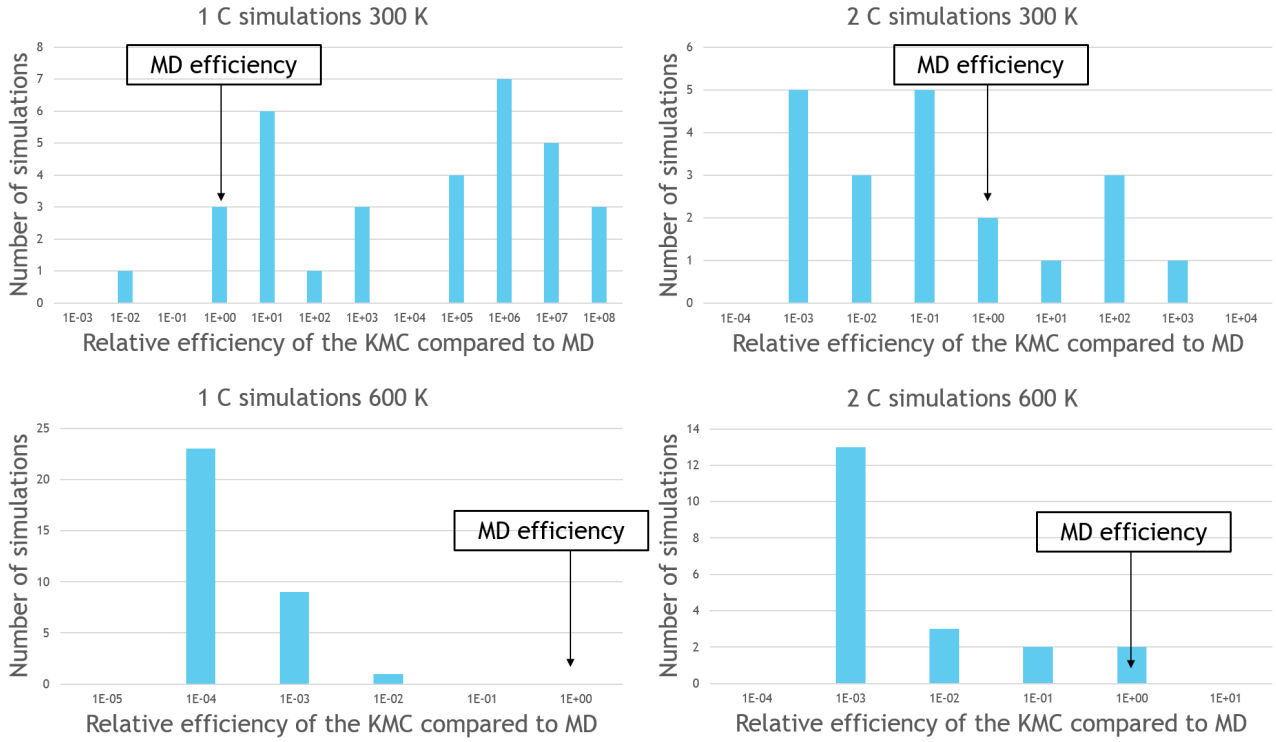

Figure 17. Relative efficiency of k-ART compared with MD for simulations with: one C atom at 300 K (a), two C atoms at 300 K (b), one C atom at 600 K (c) and two C atoms at 600 K (d).

between two C atoms. This indicates that a repulsion is occurring between the two C atoms and the loop even if the two C atoms are not directly within the loop: the loop needs a high energy in order to cross over these atoms. This can be seen on figure 7 where the C atom and the loop have a repulsing interaction even if the C atom is not within the loop.

This effect was not observed in $9 \times 9 \times 9$ simulations for two main reasons:

– the $9 \times 9 \times 9$ box is small, therefore the probability of the loop going back to the C atoms after it left is higher than in a $20 \times 20 \times 20$ and so is the probability of overcoming the energy barrier needed for the two C atoms to be in the loop again;
– as seen on figure 7, a repulsion is occurring between the loop and the C atom even if the C atom is not within the loop. In a $9 \times 9 \times 9$ box, the periodic images of C atoms help the loop to go through the C atoms in the initial box. In a $20 \times 20 \times 20$ box, the periodic images of C atoms are too far away from the loop to have an interaction with it.

4. Discussion

The interaction of solutes with interstitial loops stabilizes the i19 loop and reduce its mobility, which should slow down its growth. This is indeed observed with the effect of Mn and Ni (which have the largest concentration among other solutes in reactor pressure vessel materials) [41] in agreement with DFT calculations [14].

As seen in throughout this paper, the main effect of C atoms on loops is their pinning. The pinning time of the loop by the C atom can be estimated using an Arrhenius law with an attempt frequency equal to 10^{13} Hz, the same as the one used by k-ART:

$$\frac{1}{t} = \omega_0 \mathrm{e}^{-\left(\frac{E_\mathrm{d}}{k_\mathrm{B}T}\right)},$$

where t is the estimated average pinning time, ω_0 is the attempt frequency and $E_\mathrm{d} = E_\mathrm{b} + E_\mathrm{migC}$ is the dissociation energy of the C-loop system. It was estimated that the loop will unpin from one C atom in 6.92×10^8 s at 300 K and in 0.008 32 s at 600 K. For the C2-loop system, if we suppose that the C atoms dissociates successively from the loop and do not recombine with it, the loop will unpin from the two C atoms in 1.38×10^9 s at 300 K and in 0.0166 s at 600 K. Therefore, at 300 K, the loop will never unpin from C atoms suggesting that the C-loop and the C2-loop systems needs to interact with other defects for the loop to unpin. However, at 600 K, the unpinning of the loop can occur with no external defects influence. The C2-loop system may even be hard to form because of the low pinning time of the loop by one C atom. Note that these calculations were done using the lowest value of a dissociation energy (i.e. $E_\mathrm{d} = E_\mathrm{b} + E_\mathrm{migC} = 0.5 + 0.8 = 1.3\,\mathrm{eV}$) and that the pinning may be stronger between the loop and C atoms. This phenomenon is similar to what Veiga observed to C atoms in the vicinity of a screw dislocation [42] which have to overcome a high energy barrier to leave the dislocation. The pinning effect of C atoms can be extended to the study of the diffusion of carbon in a dislocation which is less mobile than a loop and then easier to pin (for same length defects). The main factor on the loop mobility is then related to the C concentration and more precisely the C atom placements. C atoms at the periphery of the loop will act as strong anchoring points, allowing other C atoms to come near.

Figure 17 summarizes the efficiency of the KMC and the MD methods for simulations at 300 K with one and two C atoms. The relative efficiency of the KMC compared to MD is calculated as such:

$$\eta = \frac{\text{Efficiency}_{\text{KMC}}}{\text{Efficiency}_{\text{MD}}} = \frac{\frac{\text{Simulatedtime}_{\text{KMC}}}{\text{CPUtime}_{\text{KMC}}}}{\frac{\text{Simulatedtime}_{\text{MD}}}{\text{CPUtime}_{\text{MD}}}}.$$

By looking at figure 17, one can observe the direct effect of the temperature on the relative efficiency of k-ART compared to MD: the rising of the temperature influenced only the KMC efficiency. The main reason of the lowering of the KMC efficiency can be seen in such that higher temperatures lead to higher transition rates and thus lower residence time. In order to enhance the KMC efficiency especially for high temperatures, a combination between a soft lattice where the system is distorted and a rigid lattice in the matrix can be made. Indeed, it seems wiser to develop a new method around the k-ART method than to a combination of meta-dynamics (for the thermodynamics of the system) and temperature accelerated dynamics to reach simulated times [43] of the second time scale at high temperatures.

5. Conclusions

We have determined the binding energy of a single C atom with a perfect ⟨1 1 1⟩ loop containing 19 SIA using DFT and a Fe–C empirical potential. Our results indicate that the most attractive configurations are the ones with the C atom at the external boundary of the loop (0.55 eV) because this is where they disturb the less the iron matrix and the most repulsive configurations are the ones with the C atom within the loop. Turning to kinetics, the main observation is the C atoms turning around the loop along a low-migration energy pathway at 300 K and 600 K.

At 300 K, when the C atom(s) are strongly bound to the loop, the pinning effect is so strong that the loop is never observed to go far from the C atoms in the simulation length spans (~0.2 s with one C atom and 10^{-5} s with two C atoms). When, in these configurations, the loop manages to move slightly, it drags the C atom(s) with it. At 600 K, one C atom does not provide a strong enough anchoring point to ensure that the loop will not unpin from it, however two C atoms in strong binding positions do most of the time. The dragging of the C atoms by the loop appear more often than at 300 K.

Within the short physical time simulated by accurate off lattice k-ART KMC, three possible mechanisms have been identified: unpinning of the loop from the almost immobile C atom, migration of the C atom around the loop, small motion of the loop dragging the C atom. Due to the time simulated, we have not been able to quantify these mechanisms in terms of diffusion coefficient or trapping time, indeed, the loop–C atom object is not immobile and some diffusion can be expected, as observed experimentally [44].

The k-ART method offers thus the possibility to explore complex mechanisms such as correlated migration of the SIA within the loop and the C atom migration in the distorted region around the loop. For the simulation of larger systems, k-ART needs however to be coupled to metadynamics and/or lattice KMC.

Acknowledgments

This work is part of the EM2VM (study and modelling of the microstructure for the ageing of materials) joint laboratory. This work was supported within the European project PERFORM60 and SOTERIA (661913). This work was partly supported by the MAI-sn (Materials Ageing Institute-Scientific Network (http://themai.org/scientific-network)).

It contributes to the Joint Programme on Nuclear Materials (JPNM) of the European Energy Research Alliance (EERA).

R G A Veiga gratefully acknowledges funding by FAPESP grant No. 2014/10294-4 and CAPES/COFECUB 770/13. Normand Mousseau is supported in part by the Natural Sciences and Engineering Research Council of Canada (NSERC). We are grateful for the support of Calcul Québec and Compute Canada for generous allocation of computer resources for part of this project.

DFT calculations have been performed on EDF R&D HPC resources and we also acknowledge PRACE for awarding us access to resource MARCONI-KNL based in Italy at CINECA (project MORPHO: MOdelling Radiation damage: characterization of elementary PHysical prOcesses, grant No. 2016153636).

ORCID iDs

R Candela https://orcid.org/0000-0001-8263-9462
R G A Veiga https://orcid.org/0000-0001-7035-1429

References

[1] Arakawa K *et al* 2014 One-dimensional glide motion of 'Naked' nanoscale 1/2⟨1 1 1⟩; prismatic dislocation loops in iron *ISIJ Int.* **54** 2421–4
[2] Xu H, Stoller R E, Osetsky Y N and Terentyev D 2013 Solving the puzzle of ⟨1 0 0⟩ interstitial loop formation in bcc iron *Phys. Rev. Lett.* **110** 265503
[3] Arakawa K, Hatanaka M, Mori H and Ono K 2004 Effects of chromium on the one-dimensional motion of interstitial-type dislocation loops in iron *J. Nucl. Mater.* **329–33** 1194–8
[4] Becquart C S, Domain C and Foct J 2005 *Ab initio* calculations of some atomic and point defect interactions involving C and N in Fe *Phil. Mag.* **85** 533
[5] Becquart C S *et al* 2010 Modeling the long-term evolution of the primary damage in ferritic alloys using coarse-grained methods *J. Nucl. Mater.* **406** 39–54
[6] Anento N and Serra A 2013 Carbon–vacancy complexes as traps for self-interstitial clusters in Fe–C alloys *J. Nucl. Mater.* **440** 236–42
[7] Terentyev D *et al* 2011 Interaction of carbon with vacancy and self-interstitial atom clusters in α-iron studied using metallic–covalent interatomic potential *J. Nucl. Mater.* **408** 272–84
[8] Terentyev D, Anento N and Serra A 2012 Interaction of dislocations with carbon-decorated dislocation loops in bcc Fe: an atomistic study *J. Phys.: Condens. Matter* **24** 455402
[9] Tapasa K, Barashev A V, Bacon D J and Osetsky Y N 2007 Computer simulation of the interaction of carbon atoms

with self-interstitial clusters in α-iron *J. Nucl. Mater.* **361** 52–61
[10] Chockalingam K, Janisch R and Hartmaier A 2014 Coupled atomistic-continuum study of the effects of C atoms at α-Fe dislocation cores *Model. Simul. Mater. Sci. Eng.* **22** 075007
[11] Khater H A, Monnet G, Terentyev D and Serra A 2014 Dislocation glide in Fe–carbon solid solution: from atomistic to continuum level description *Int. J. Plast.* **62** 34–49
[12] Cottrell A H and Bilby B A 1949 Dislocation theory of yielding and strain ageing of iron *Proc. Phys. Soc.* A **62** 49
[13] Veiga R G A, Goldenstein H, Perez M and Becquart C S 2015 Monte Carlo and molecular dynamics simulations of screw dislocation locking by Cottrell atmospheres in low carbon Fe–C alloys *Scr. Mater.* **108** 19–22
[14] Domain C and Becquart C S 2018 Solute–$\langle 1\,1\,1\rangle$ interstitial loop interaction in α-Fe: a DFT study *J. Nucl. Mater.* **499** 582–94
[15] Becquart C S *et al* 2007 Atomistic modeling of an Fe system with a small concentration of C *Comput. Mater. Sci.* **40** 119–29
[16] Kresse G and Hafner J 1993 *Ab initio* molecular dynamics for liquid metals *Phys. Rev.* B **47** 558–61
[17] Kresse G and Hafner J 1994 Norm-conserving and ultrasoft pseudopotentials for first-row and transition elements *Condens. Matter* **6** 8245–57
[18] Kresse G and Hafner J 1994 *Ab initio* molecular-dynamics simulation of the liquid-metal–amorphous-semiconductor transition in germanium *Phys. Rev.* B **49** 14251
[19] Kresse G and Joubert D 1999 From ultrasoft pseudopotentials to the projector augmented-wave method *Phys. Rev.* B **59** 1758
[20] Perdew J P *et al* 1992 Atoms, molecules, solids, and surfaces: applications of the generalized gradient approximation for exchange and correlation *Phys. Rev.* B **46** 6671
[21] Varvenne C, Bruneval F, Marinica M-C and Clouet E 2013 Point defect modeling in materials: coupling *ab initio* and elasticity approaches *Phys. Rev.* B **88** 134102
[22] Becquart C S *et al* 1997 Massively parallel molecular dynamics simulations with EAM potentials *Radiat. Eff. Defects Solids* **142** 9–21
[23] Veiga R G A, Becquart C S and Perez M 2014 Comments on 'Atomistic modeling of an Fe system with a small concentration of C' *Comput. Mater. Sci.* **82** 118–21
[24] Clouet E, Garruchet S, Nguyen H, Perez M and Becquart C S 2008 Dislocation interaction with C in α-Fe: a comparison between atomic simulations and elasticity theory *Acta Mater.* **56** 3450–60
[25] Veiga R G A, Perez M, Becquart C S, Clouet E and Domain C 2011 Comparison of atomistic and elasticity approaches for carbon diffusion near line defects in α-iron *Acta Mater.* **59** 6963–74
[26] Restrepo O A *et al* 2016 Diffusion properties of Fe–C systems studied by using kinetic activation–relaxation technique *Comput. Mater. Sci.* **112** 96–106
[27] Garruchet S and Perez M 2008 Modelling the carbon snoek peak in ferrite: coupling molecular dynamics and kinetic Monte-Carlo simulations *Comput. Mater. Sci.* **43** 286–92
[28] Gunkelmann N, Ledbetter H and Urbassek H M 2012 Experimental and atomistic study of the elastic properties of α' Fe–C martensite *Acta Mater.* **60** 4901–7
[29] Sinclair C W, Perez M, Veiga R G A and Weck A 2010 Molecular dynamics study of the ordering of carbon in highly supersaturated α-Fe *Phys. Rev.* B **81** 224204
[30] Domain C, Becquart C S and Foct J 2004 *Ab initio* study of foreign interstitial atom (C, N) interactions with intrinsic point defects in α-Fe *Phys. Rev.* B **69** 144112
[31] El-Mellouhi F, Mousseau N and Lewis L J 2008 Kinetic activation-relaxation technique: an off-lattice self-learning kinetic Monte Carlo algorithm *Phys. Rev.* B **78** 153202
[32] Béland L K, Brommer P, El-Mellouhi F, Joly J-F and Mousseau N 2011 Kinetic activation-relaxation technique *Phys. Rev.* E **84** 046704
[33] McKay B D 1981 Practical graph isomorphism *Congr. Numer.* **30** 45
[34] Barkema G T and Mousseau N 1996 Event-based relaxation of continuous disordered systems *Phys. Rev. Lett.* **77** 4358
[35] Malek R and Mousseau N 2000 Dynamics of Lennard-Jones clusters: a characterization of the activation-relaxation technique *Phys. Rev.* E **62** 7723
[36] Hepburn D J and Ackland G J 2008 Metallic-covalent interatomic potential for carbon in iron *Phys. Rev.* B **78** 165115
[37] Ventelon L *et al* 2015 Dislocation core reconstruction induced by carbon segregation in bcc iron *Phys. Rev.* B **91** 220102
[38] Ackland G J, Mendelev M I, Srolovitz D J, Han S and Barashev A V 2004 Development of an interatomic potential for phosphorus impurities in α-iron *J. Phys.: Condens. Matter* **16** S2629
[39] Johnson R A, Dienes G J and Damask A C 1964 Calculations of the energy and migration characteristics of carbon and nitrogen in α-iron and vanadium *Acta Metall.* **12** 1215–24
[40] Domain C and Monnet G 2005 Simulation of screw dislocation motion in iron by molecular dynamics simulations *Phys. Rev. Lett.* **95** 215506
[41] Hernández-Mayoral M and Gómez-Briceño D 2010 Transmission electron microscopy study on neutron irradiated pure iron and RPV model alloys *J. Nucl. Mater.* **399** 146–53
[42] Veiga R G A 2011 Computational insights into the strain aging phenomenon in bcc iron at the atomic scale *PhD Thesis* INSA de Lyon
[43] Sorensen M R and Voter A F 2000 Temperature-accelerated dynamics for simulation of infrequent events *J. Chem. Phys.* **112** 9599–606
[44] Arakawa K *et al* 2007 Observation of the one-dimensional diffusion of nanometer-sized dislocation loops *Science* **318** 956–9